Copy
RM L57E10a

615

NACA

CASE FILE COPY

RESEARCH MEMORANDUM

DESIGN AND EVALUATION OF A TURBOJET-EXHAUST SIMULATOR

WITH A SOLID-PROPELLANT ROCKET MOTOR

FOR FREE-FLIGHT RESEARCH

By Abraham Leiss

Langley Aeronautical Laboratory
Langley Field, Va.

NATIONAL ADVISORY COMMITTEE
FOR AERONAUTICS

WASHINGTON

July 5, 1957

CONFIDENTIAL

NATIONAL ADVISORY COMMITTEE FOR AERONAUTICS

RESEARCH MEMORANDUM

DESIGN AND EVALUATION OF A TURBOJET-EXHAUST SIMULATOR

WITH A SOLID-PROPELLANT ROCKET MOTOR

FOR FREE-FLIGHT RESEARCH

By Abraham Leiss

SUMMARY

A turbojet-exhaust simulator with a sonic exit, powered with a solid-propellant rocket motor was designed and tested in both cold air and under actual combustion conditions. The exit pressure ratio of the simulator was designed to simulate the exit pressure ratio of a current turbojet engine. The simulator was developed by so changing the internal-flow configuration that the high energy of the rocket motor was reduced sufficiently to produce a lower energy sonic exit. A satisfactory simulator was developed after nine configurations were tunnel tested. Five of of these tunnel-test configurations produced a supersonic exit. Of the four tunnel-test configurations with a sonic exit, one was chosen for its best overall qualities and tested further with the solid-propellant rocket motor.

Included in the results are the effects of an internal-flow step, change of divergence angle, change of convergence angle, and use of a shock bar in the flow field. The shock bar was found to be necessary to produce the required energy loss if the length of the simulator is to remain practical.

INTRODUCTION

It is shown in references 1 to 8 that a propulsive jet can have an appreciable interference effect on the external aerodynamics of airplane and missile configurations. The rocket motors, used in the turbojet simulator developed in reference 9 and used to produce the power in references 5 to 8, had low combustion-chamber pressures. In order to produce a sonic exit with a turbojet simulator from these low-pressure combustion-chamber rocket motors, a straightforward mathematical design was satisfactory. This turbojet simulator, as designed in reference 9, became obsolete when the supply of SU/K cordite solid-propellant grains

CONFIDENTIAL

was exhausted. Since the cordite rocket motors are no longer available, a substitute motor had to be used and a simulator designed for that particular rocket motor. The rocket motors JATO, 5-KS-900, (T44) that are available for future testing are high-pressure motors having chamber pressures of the order of 100 atmospheres. For such high chamber pressures, the losses in energy required and the possibility of large turbulence in a simulator of relatively short length necessitated the undertaking of an exploratory investigation of the effect of the internal geometric structure between the first and second minimum sections of the simulator.

A turbojet-exhaust simulator, designed for air tunnel testing was constructed from interchangeable parts, so that various internal-flow configurations could be formed. Nine such flow configurations were assembled from the simulator components. These nine general configurations consisted of two basic changes in the design: (1) the shape of the internal walls and (2) obstructions to the internal-flow path. Twelve tunnel tests were made of these nine configurations. Upon selection of a satisfactory turbojet simulator that had the required exit pressure ratio (that is, the same as the turbojet engine simulated), a T44 rocket motor was attached and ground tested as final proof that the configuration would be satisfactory.

SYMBOLS

a to i	exhaust-simulator orifice designations
A to Z	tunnel-test orifice designations
A	local cross-sectional area
D	diameter
F	thrust
M	Mach number
p	static pressure
p'	total pressure
p_e	calculated jet exit pressure, $\dfrac{0.5283 A_T p'_t}{A_e}$
R	gas constant

t   time

T   temperature

γ ratio of specific heats

ρ density

Subscripts:

A   at orifice station A (near exit)

c   combustion chamber

e   exit

p   plenum chamber

t   tunnel settling chamber

T   throat

∞ free stream

DESIGN CONSIDERATIONS

Since the turbojet simulator of reference 9 is no longer available, a turbojet simulator design for the JATO, 5-KS-900, T44 rocket motor is required. The T44 rocket motor is equipped with a T-14E1 solid-propellant grain. Rocket motor and grain data obtained from references 10 and 11 are as follows:

$$\gamma = 1.27$$

$$T_c = 3421^\circ \text{ R}$$

$$\rho = 0.0572 \text{ lb/cu in.}$$

$$p'_c = 1815 \text{ lb/sq in., abs}$$

$$t = 5.9 \text{ sec   at } 70^\circ \text{ F}$$

As discussed in reference 9, the primary parameters to be considered in the design of a turbojet simulator are the jet thrust, the jet weight flow relative to the free-stream weight flow, and the jet total pressure relative to the free-stream static pressure. Thus, successful design of a small rocket motor operating to simulate a full-scale turbojet engine depends upon the ability to obtain exhaust parameters γ_e/γ_∞, p_e/p_∞, M_e/M_∞, and $\sqrt{R_\infty T_\infty/R_e T_e}$ equal to those of the full-scale turbojet exhaust, for the condition when the free-stream Mach number of the rocket motor is the same as that of the turbojet engine. The parameters γ_e/γ_∞ and $\sqrt{R_\infty T_\infty/R_e T_e}$ of the T44 rocket motor roughly simulate these parameters for the turbojet engine. The parameter M_e/M_∞ is simulated by use of a choking exit and by maintaining the free-stream Mach number the same as for the turbojet engine. The p'_e/p_∞ is simulated by dissipating the high pressure of the T44 rocket exhaust through a double-throated nozzle designed to give the required pressure ratio at the simulator exit. For the purposes of design, the operating characteristics of the turbojet engine (with afterburner operating) are assumed to be:

$$p'_e/p_\infty = 5.97$$

$$M_e = 1.00$$

$$M_\infty = 1.40$$

$$\text{Altitude} = 4{,}000 \text{ ft}$$

The exit area and the plenum-chamber area (minimum area required to hold a normal shock) were obtained by assuming one-directional isentropic flow and derived as follows:

$$A_T = \frac{\pi D_T^2}{4} = \frac{\pi (0.820)^2}{4} = 0.528 \text{ sq in.}$$

$$p'_e = p_\infty(\text{at } 4{,}000 \text{ ft}) \times \frac{p'_e}{p_\infty} = 12.7 \times 5.97 = 75.8 \text{ lb/sq in., abs}$$

$$\frac{p'_e}{p'_c} = \frac{75.8}{1815} = 0.0415$$

From formulas given in reference 12,

$$M_p = f\left[\left(\frac{p'_e}{p'_c}\right), \gamma\right] = 4.67$$

$$\frac{A_p}{A_T} = f\left[\left(M_p\right), \gamma\right] = 39.6$$

$$A_p = \frac{A_p}{A_T} A_T = 39.6 \times 0.528 = 20.9 \text{ sq in.}$$

$$D_p = \sqrt{\frac{4A_p}{\pi}} = 5.15 \text{ in. (minimum)}$$

In order to insure stable flow, a value of $D_p = 5.5$ inches is used. Then

$$A_e = \frac{p'_c A_T}{p'_e} = \frac{1815 \times 0.528}{75.8} = 12.57 \text{ sq in.}$$

$$D_e = \sqrt{\frac{4A_e}{\pi}} = 4.00 \text{ in.}$$

A tunnel-test model was designed and built to these dimensions, as shown in figures 1 and 2. It was decided, for reasons of economy and instrumentation, to construct a cold-air tunnel-test model rather than to test fire solid-propellant rocket motors until a satisfactory configuration was developed. The tunnel-test model was constructed so that the simulator could easily be varied in internal geometry by interchanging the component parts between test runs. Equipment for nine test configurations was built.

APPARATUS AND TESTS

Tunnel-Test Model

The test simulator was installed in a high-pressure tunnel of the Gas Dynamics Branch at the NACA Langley Aeronautical Laboratory. The tunnel is of the direct-blowdown type, that is, dry air from the storage tank passes directly through the simulator and exhausts into the atmosphere. The dry air temperature in the tunnel settling chamber was 100° F. Two valves in the supply line, a manually controlled gate valve and an automatic pressure-regulating valve, are used to maintain constant stagnation pressure. Downstream of the valves is a 14-inch-diameter settling chamber approximately 3 feet long as illustrated in figure 3. Installed in the central part of the chamber to improve the uniformity of the flow are two 30- by 30-mesh bronze screens (0.009-inch-diameter wire), spaced 3/4 inch apart. Attached to the settling chamber is a heavy flange, sketched in figure 1 containing the throat of the simulator.

The nozzle throat was faired into the plenum chamber with a divergent detachable cylinder as shown in figure 1. Two divergent sections were built. The 45° divergent section was 3.78 inches long, and the 22.9° divergent section was 7.70 inches long. The 45° and 22.9° divergent sections were installed and used in five and six tests, respectively. One tunnel test was made without any divergent section.

Two diffusers were built. The first was 16 inches long with a 5.37° convergence angle and a 4-inch exit diameter and the second was 10.5 inches long with an 8.17° convergence angle and a 4-inch exit diameter. The 5.37° diffuser had 15 static-pressure orifices. The 8.17° diffuser had 10 static-pressure orifices. The orifices located on the convergent part of the diffusers were evenly spaced. Each diffuser was attached to the nozzle flange with a plenum-chamber section in-between.

A flanged total-pressure rake was installed between the plenum chamber and diffuser. An exit rake was also used. As shown in figures 1 and 5, a static-pressure rake was installed at the exit for one of the twelve test runs, a total-pressure rake was used for five test runs, and a combination rake (three static-pressure tubes and one total-pressure tube) was used for three test runs. Three test runs were made without a rake at the exit.

Static and total pressures were measured on 16-inch-dial gages of the precision Bourdon type which had ranges of 0 to 50, 0 to 100, 0 to 150, 0 to 200, 0 to 500, and 0 to 2,000 lb/sq in. The gage with a range of 0 to 2,000 lb/sq in. was connected to the tunnel settling chamber. These gages, shown in figure 4, are accurate to within ±0.5 percent of full-scale deflection and are not intended for measuring pressures less than ambient pressure, although such values between 0 and -10 lb/sq in. could be estimated.

CONFIDENTIAL

The pressure gages were intermittently photographed and the pressures were read directly from the photographs. The pressure gages were photographed, after the tunnel-settling-chamber pressure had damped out, at intervals of 100 lb/sq in. from 500 lb/sq in. to approximately 1,800 lb/sq in.

Twelve tests were made with the divergence angle, the plenum-chamber dimensions, and the convergence angle varied and with a stream-disturbance bar, called a shock bar, installed. The throat and exit diameters remained constant for all test runs. Figure 5 illustrates the 12 configurations used for the tunnel tests and shows the positions of the orifices. In table I are given the internal-flow areas at each static-pressure orifice. Pertinent dimensions for the test configurations are shown in table II. Because of the many variables considered, it was possible to make 15 configuration comparisons as outlined in table III.

For tunnel tests IV, XI, and XII a steel bar, $\frac{1}{2}$ inch by 1 inch by 5.5 inches, was welded in the plenum chamber as shown in figure 6.

Rocket Model

The geometric configuration of tunnel test IV (fig. 5) was used to build a simulator that would attach to the rocket motor. Figure 7 shows a photograph of this simulator. The sketch of figure 8 shows the complete T44 rocket motor with simulator. The simulator was designed and built with the 5.37° convergent diffuser and the 22.9° divergent fairing. A $\frac{1}{2}$- by 1-inch steel bar was welded between the divergent and convergent sections as shown in figure 8. Eight static-pressure orifices spaced as shown in figure 8 comprised the rocket-simulator pressure instrumentation. The rocket combustion-chamber pressure was also measured.

Two rocket-motor tests of the simulator (with and without the shock bar) were made at the Langley rocket test cell. These rocket tests were primarily check tests to substantiate the results of the tunnel tests. Shown in figure 9 is the rocket motor with simulator mounted on a thrust stand in the rocket test cell. The thrust produced by the rocket motor was measured by an electrical strain gage and registed on a recording galvanometer. All the pressures were measured with Statham gages. A timer incorporated in the recording system provides a time history of thrust and pressure measurements.

RESULTS AND DISCUSSION

Tunnel-Test Results

Pressure distributions.- Figure 10 presents the static-pressure distribution along the turbojet simulator wall of tunnel total pressure for all tests with a sonic exit. The static pressures for the test with supersonic exits could not be measured (negative gage pressures) with the Bourdon gages. The configuration for test VII converted to a supersonic exit for tunnel total pressures greater than 1,200 lb/sq in., abs, and therefore no pressure measurements could be obtained. The statistical data of the other four tests with supersonic exits are included in table II. The orifice designations in figure 10 correspond to the orifices A to Z shown in figure 5.

A comparison of the pressure distributions in the convergent part of the simulators for the tests shown in figure 10 indicates that the flow was fairly smooth in all cases except in tests XI and XII. In tests I, II, IV, V, VI, and VII, the convergent section apparently acted as a supersonic diffuser to decelerate the flow through reflected oblique shocks to a weak normal shock at stations corresponding to the maximum static pressures. After the weak normal shock, the flow became subsonic and the convergent section acted as a subsonic effuser to accelerate the flow to Mach number 1.0 at the exit. The ratio of the static pressure at the wall to the calculated static pressure at the exit p/p_e was averaged for each tunnel-test configuration and the variation of these average ratios with the ratio of the area at each station to the area at the exit A/A_e for various sonic-exit configurations is presented in figures 11 to 14.

Effect of shock bar.- Test III was made without the plenum-chamber total-pressure rake and produced a supersonic exit. The rake had acted as a shock bar in tests I and II, since these exits were sonic. Since test III developed a supersonic exit and the rake was not used, test IV was made with the same internal geometry as test III plus the addition of a shock bar. The result was a sonic exit. Tests III and IV had 5.37° convergent sections. The same tests were made with the 8.17° convergent section and, as previously, the configuration with the shock bar (test XI) produced a sonic exit and without the shock bar (test IX) yielded a supersonic exit.

The shock bar, 0.5 inch by 1.25 inch by 5.5 inches or the plenum-chamber rake, which had about the same frontal area as the shock bar, was found to be necessary to produce the high energy loss for the configurations tested. A sonic exit could conceivably be produced without a shock bar, if the length of the convergent section were not limited by practical considerations. The possibility of using an internal step instead of the

shock bar was explored in test X and was found unsatisfactory, since the type of internal step tested (fig. 5, test X) resulted in a supersonic exit.

Effect of changing divergence angle.- The 45° divergent section was installed in five tests and the 22.9^O divergent section was installed in six tests. Figure 10 indicates that the tests with the 22.9^O divergent section had a more uniform static-pressure distribution than the tests with the 45° divergent section since a sonic exit could be obtained with either divergence angle. The divergence angle obviously had little effect on the exit Mach number. (See fig. 5 and table III.) However, omitting the divergent fairing and passing the air directly into the plenum chamber in test VIII caused a supersonic exit. Since the configuration of test VI had a sonic exit and had similar design rearward of the plenum chamber to the configuration of test VIII, with the addition of the 45° divergent section, it can be concluded that the divergent section helped produce the necessary energy loss for a sonic exit. Removing the plenum chamber used in the configuration of test V, as shown in figure 5, for test VI reduced the wall static pressures. Figure 11 illustrates this effect in a plot of p/p_e against A/A_e for tests V and VI. The reduction in exit static-pressure ratio p/p_e is almost linear for area ratios A/A_e above 1.2.

The simulator length effect was considered important and was determined by varying the angles of the divergent and convergent sections. Figure 12 shows the effect of decreasing the divergence angle from 45° to 22.9^O. Although test I was made with a static-pressure rake and test IV with a total-pressure rake at the exit, it is believed that the difference in the two curves of figure 12(a) is representative of the effect due to a decrease in the divergence angle. The same applies to tests VI and XI (fig. 12(b)). Tests VII and XII (fig. 12(c)) show the effect of decreasing the divergence angle without exit-rake interference.

Effect of changing convergence angle.- Two convergent sections were used in the investigation. Figure 13 presents the effect of increasing the convergence angle from 5.37^O to 8.17^O. Tests I to IV were made with the 5.37^O convergent section and tests V to XII were made with the 8.17^O convergent section. Tests I and V are comparable since their configurations were similar except for the change in convergent sections. As illustrated in figure 13, an increase in the convergence angle or a decrease in the convergent section length (tests I and V) decreased the wall static pressures. This pressure decrease can also be seen when results of tests II and VII, as well as tests IV and XI, are compared. Internal flow for test IV was smoother than for test XI. Tests III and IX used comparable configurations, since the only difference was in the convergence of the sections; however, both tests developed supersonic exits because of the lack of a shock bar.

When results from tests II and VII were compared (fig. 13(b)), the 5.37^O convergent section was preferred to the 8.17^O convergent section

because the configuration of test VII was considered too critical to pro-
duce a sonic exit for the complete pressure range.

Effect of exit rake.- The exit rake was used to survey the flow at
the exit in nine tests. The exit rake is not part of the permanent con-
figuration and therefore tests were made without the exit rake in order
to determine the effect of the reduction in area due to the exit rake.
Figure 14 shows the interference effects caused by the exit rake.
Test I, which had a sonic exit, was made with a static-pressure exit
rake. Test II used the same configuration as test I, but the static-
pressure exit rake was eliminated. Both tests had sonic exits but the
ratio p/p_e at the exit was less for test II (fig. 14(a)). The exit
rake caused slightly higher wall static pressures as is evident in fig-
ure 10 for tests I and XI.

The combination exit pressure rake of test VI was removed and
test VII made. Also, the total-pressure exit rake of test XI was
removed and test XII was made. Removing the exit rakes from tests VI
and XI caused lower wall static pressures in tests VII and XII, respec-
tively, as well as in test II. However, in tests II and VII the pres-
sures near the exit were lower, but the pressures at the upstream end
of the convergent section were increased when the exit rake was removed.
Removing the rake from the configuration of test VI not only increased
the pressure over a larger area of the convergent section (test VII) but
also resulted in a supersonic exit for all values of $p'_t < 1200$. (See
fig. 14(b).) Since the configuration of test VII cannot produce a sonic
exit at the higher values of p'_t, the configurations of tests VI and VII
were considered unsatisfactory to produce the necessary loss of energy.
The exit rake of test I was a static-pressure rake, the exit rake of
test XI was a total-pressure rake, and the exit rake of test VI had three
static-pressure tubes and one total-pressure tube.

Analysis.- For test I, the plenum-chamber rake support acted as a
shock bar, and created turbulence in the flow. This turbulence was
smoothed out somewhat as the air passed through the convergent part of
the simulator (fig. 15). Presented in figure 15 is a survey of the
plenum chamber and exit pressures as measured by the total-pressure rake
in the plenum chamber and by the static-pressure rake at the exit for the
complete range of tunnel pressures. These rake-pressure-survey measure-
ments for most of the tunnel tests are given in table IV.

The three configurations of tests I, IV, and XII produced sonic
exits and could be used with the solid-propellant rocket to produce a
turbojet simulator. Since test I had the 45° divergent section, which
was considered less favorably than the 22.9° divergent section, and since
test XII had the 8.17° convergent section, which was found to be less
favorable than the 5.37° convergent section, because of the results of

test VII, the configuration chosen as the best for the rocket tests was that of test IV with the 22.9° divergent section and the 5.37° convergent section.

Rocket Motor Results

The simulator configurations used in the Langley rocket test all were similar to the configurations of tunnel air test IV. Figure 16 presents the variation of combustion pressure and thrust with time for the two T44 rocket-simulator tests. The configuration difference in the two tests resulted from the installation of a shock bar. The results for the tests with the shock bar show slightly lower combustion-chamber pressures than that without the shock bar; however, the thrust for the test without the shock bar was much higher and also produced a supersonic exit. Figure 17 presents the variation of static pressure with combustion pressure for each orifice measurement on the T44 turbojet simulator. The curves are for the data of the test with a shock bar between the convergent and divergent sections. All of the orifices had a similar rate of pressure rise with an increase in combustion pressure. Figure 18 presents the variation of static-pressure distribution with exit-area ratio for the T44 turbojet simulator with the shock bar. These pressures are slightly lower than the pressures obtained in tunnel test IV (fig. 13(c)). Since the test with the shock bar installed in the T44 turbojet simulator produced a smooth working, sonic exit rocket motor with the required exit total-pressure-ratio range, this configuration was selected for use in jet-effect free-flight tests.

Figure 19 presents the exit total-pressure ratios required, actual $\left(p'_A/p_A\right)$ and calculated $\left(p'_A/p_e\right)$ as a function of tunnel settling-chamber total pressure for tunnel test IV. This shows that a sonic exit exists.

CONCLUDING REMARKS

From tunnel tests and rocket-cell tests of several configurations, a satisfactory turbojet simulator was produced for use with solid-propellant rocket motors; however, a shock bar was required to produce a sonic exit in order that the length of the convergent section remain practical.

Langley Aeronautical Laboratory,
      National Advisory Committee for Aeronautics,
            Langley Field, Va., May 3, 1957.

REFERENCES

1. Bressette, Walter E.: Investigation of the Jet Effects on a Flat
   Surface Downstream of the Exit of a Simulated Turbojet Nacelle at
   a Free-Stream Mach Number of 2.02. NACA RM L54E05a, 1954.

2. Cortright, Edgar M., Jr., and Kochendorfer, Fred D.: Jet Effects on
   Flow Over Afterbodies in Supersonic Stream. NACA RM E53H25, 1953.

3. Bressette, Walter E., and Leiss, Abraham: Investigation of Jet Effects
   on a Flat Surface Downstream of the Exit of a Simulated Turbojet
   Nacelle at a Free-Stream Mach Number of 1.39. NACA RM L55L13, 1956.

4. Leiss, Abraham, and Bressette, Walter E.: Pressure Distribution
   Induced on a Flat Plate by a Supersonic and Sonic Jet Exhaust at a
   Free-Stream Mach Number of 1.80. NACA RM L56I06, 1957.

5. Leiss, Abraham: Free-Flight Investigation of Effects of Simulated
   Sonic Turbojet Exhaust on the Drag of Twin-Jet Boattail Bodies at
   Transonic Speeds. NACA RM L56D30, 1956.

6. Falanga, Ralph A.: A Free-Flight Investigation of the Effects of
   Simulated Sonic Turbojet Exhaust on the Drag of a Boattail Body With
   Various Jet Sizes From Mach Number 0.87 to 1.50. NACA RM L55F09a,
   1955.

7. Falanga, Ralph A.: A Free-Flight Investigation of the Effects of a
   Sonic Jet on the Total-Drag and Base Pressure Coefficients of a
   Boattail Body of Revolution From Mach Number 0.83 to 1.70. NACA
   RM L55L21, 1956.

8. Falanga, Ralph A., and Leiss, Abraham: Free-Flight Investigation at
   Transonic Speeds of Drag Coefficients of a Boattail Body of Revolu-
   tion With a Simulated Turbojet Exhaust Issuing at the Base From
   Conical Short-Length Ejectors.   NACA RM L56H23, 1956.

9. DeMoraes, Carlos A., Hagginbothom, William K., Jr., and Falanga,
   Ralph A.: Design and Evaluation of a Turbojet Exhaust Simulator
   Utilizing a Solid-Propellant Rocket Motor, for Use in Free-Flight
   Aerodynamic Research Models. NACA RM L54I15, 1954.

10. Higginson, John: Notes on Development of JATO, 5-KS-900, T-44. Rep.
    No. 5-51 (Contract No. W-36-034-ORD-7709, ORD Project TU2-2025),
    Thiokol Corp., Redstone Div. (Huntsville, Ala.), Feb. 1951.

11. Anon: JATO Manual. Vol. II - JATO Units of Current Interest.
    SPIA/Mlb, Unit 106 (Contract NOrd 7386), The Johns Hopkins Univ.,
    Appl. Phys. Lab., Sept. 1956.

12. Ames Research Staff: Equations, Tables, and Charts for Compressible
    Flow. NACA Rep. 1135, 1953. (Supersedes NACA TN 1428.)

TABLE I.- SIMULATOR DIMENSIONS AT ORIFICE STATIONS

Static-pressure orifice	Distance from exit, in.	Internal diameter, in.	Internal area, sq. in.
5.37° convergence			
A	0.125	4.000	12.566
B	.740	4.022	12.705
C	1.739	4.116	13.305
D	2.738	4.210	13.920
E	3.737	4.303	14.542
F	4.736	4.397	15.185
G	5.735	4.491	15.841
H	6.734	4.588	16.533
I	7.733	4.678	17.188
J	8.732	4.772	17.885
K	9.730	4.865	18.589
L	10.729	4.959	19.314
M	11.728	5.053	20.054
N	12.727	5.146	20.798
O	13.726	5.240	21.565
P	18.563	5.500	23.758
Q	21.313	5.500	23.758
8.17° convergence			
A	0.125	4.000	12.566
R	.768	4.038	12.806
S	1.765	4.181	13.730
T	2.763	4.323	14.678
U	3.760	4.466	15.665
V	4.757	4.608	16.677
W	5.755	4.751	17.728
X	6.752	4.893	18.803
Y	7.750	5.036	19.918
Z	8.747	5.178	21.058
P	13.003	5.500	23.758
Q	13.753	5.500	23.758

TABLE II.- GEOMETRIC CHARACTERISTICS OF TEST CONFIGURATIONS

Test	Length (throat to exit, in.)	Divergence angle, deg	Convergence angle, deg	Tunnel pressure range, lb/sq in., abs	Exit velocity
I	30.25	45	5.37	527 to 1820	Sonic
II	30.25	45	5.37	815 to 1817	Sonic
III	28.94	22.9	5.37	535 to 705	Supersonic
IV	30.25	22.9	5.37	635 to 1820	Sonic
V	24.75	45	8.17	535 to 1825	Sonic
VI	22.00	45	8.17	525 to 1815	Sonic
VII	22.00	45	8.17	535 to 1115	Sonic-supersonic
VIII	22.00	None	8.17	535 to 640	Supersonic
IX	23.44	22.9	8.17	535 to 1335	Supersonic
X	23.44	22.9	Wedge	535 to 725	Supersonic
XI	24.75	22.9	8.17	545 to 1825	Sonic
XII	24.75	22.9	8.17	815 to 1815	Sonic

TABLE III.- EFFECTS ILLUSTRATED BY CONFIGURATION CHANGES

Test		Test		Effect of
I	45° divergence 5.37° convergence With exit rake	II	45° divergence 5.37° convergence Without exit rake	Exit rake
I	45° divergence 5.37° convergence	IV	22.9° divergence 5.37° convergence	Divergence
I	45° divergence with straight section 5.37° convergence	V	45° divergence 8.17° convergence	Convergence
II	45° divergence 5.37° convergence With plenum chamber	VII	45° divergence 8.17° convergence Without plenum chamber	Convergence and straight section
III	22.9° divergence 5.37° convergence Without shock bar	IX	22.9° divergence 8.17° convergence Without shock bar	Convergence and smooth transition
III	22.9° divergence 5.37° convergence Without shock bar	IV	22.9° divergence 5.37° convergence With shock bar	Shock bar
IV	22.9° divergence 5.37° convergence With shock bar	XI	22.9° divergence 8.17° convergence With shock bar	Convergence
V	45° divergence 8.17° convergence With plenum chamber	VI	45° divergence 8.17° convergence Without plenum chamber	Straight section
VI	45° divergence 8.17° convergence With exit rake	VII	45° divergence 8.17° convergence Without exit rake	Exit rake
VI	45° divergence 8.17° convergence	VIII	Without divergence 8.17° convergence	No divergence
VI	45° divergence 8.17° convergence	XI	22.9° divergence 8.17° convergence	Divergence
VII	45° divergence 8.17° convergence	XII	22.9° divergence 8.17° convergence	Divergence
IX	22.9° divergence 8.17° convergence Smooth transition	X	22.9° divergence 8.17° convergence With internal step	Internal step
IX	22.9° divergence 8.17° convergence Without shock bar	XI	22.9° divergence 8.17° convergence With shock bar	Shock bar
XI	22.9° divergence 8.17° convergence With exit rake	XII	22.9° divergence 8.17° convergence Without exit rake	Exit rake

TABLE IV.- RAKE PRESSURES

(a) Test II

p'_t, lb/sq in., abs	p'_p, lb/sq in., abs, at radius (in.) of -					
	0	0.5	1.0	1.5	2.0	2.5
815	71.7	200.7	91.2	20.7	11.7	11.7
925	65.7	221.7	114.7	22.2	13.2	13.7
1015	72.7	241.7	122.7	24.7	14.7	14.7
1125	73.7	261.7	136.7	26.7	15.7	16.7
1215	74.7	277.7	149.7	29.6	16.7	17.7
1365	79.7	304.7	164.7	31.7	17.7	18.7
1422	87.7	320.7	169.7	34.7	19.7	19.7
1517	89.2	338.7	184.7	35.7	21.7	21.2
1615	93.2	355.2	200.7	38.7	22.5	22.7
1715	99.7	382.7	212.7	41.7	24.2	24.7
1817	99.7	394.2	233.2	45.2	25.2	25.0

(b) Test III

p'_t, lb/sq in., abs	p'_A, lb/sq in., abs, at radius (in.) of -			
	0	0.5	1.0	1.5
535	45.9	43.7	40.7	26.7
635	51.7	56.5	61.2	28.6
705	53.7	68.7	82.2	28.1

TABLE IV.- RAKE PRESSURES - Continued

(c) Test IV

p't, lb/sq in., abs	p'A, lb/sq in., abs, at radius (in.) of -			
	0	0.5	1.0	1.5
635	27.2	27.2	28.2	28.7
725	30.7	30.7	31.2	32.2
835	34.7	34.7	35.7	37.2
925	38.2	38.6	39.2	41.2
1015	42.1	42.1	43.2	45.7
1125	46.1	46.7	48.1	49.9
1225	50.2	50.7	51.9	54.2
1325	54.2	54.7	55.7	58.6
1425	58.4	58.7	60.7	62.7
1515	62.4	62.7	64.7	67.0
1615	66.2	66.9	68.7	72.2
1735	70.7	71.7	73.7	76.2
1820	74.6	74.7	78.2	80.4

(d) Test V

p't, lb/sq in., abs	Rake pressures, lb/sq in., abs, at radius (in.) of -									
	0	0.5	1.0	1.5	2.0	2.5	0	0.5	1.0	1.5
	p'p						pA			p'A
535	60.7	120.7	63.7	14.7	7.7	6.7	17.2	17.2	15.7	33.7
635	74.7	147.7	76.7	19.7	9.7	9.7	20.2	19.7	19.2	39.6
715	94.7	168.7	86.7	20.7	11.7	14.7	23.2	23.7	22.7	41.2
825	92.7	194.7	95.7	22.7	14.7	14.7	26.6	26.7	25.2	49.7
925	109.7	214.7	111.7	25.7	14.7	14.7	29.7	29.6	27.7	54.7
1015	114.7	232.7	119.7	28.7	15.7	16.7	31.9	31.6	30.7	59.7
1115	96.7	258.7	134.7	29.7	17.7	18.7	35.2	34.7	32.7	67.1
1235	124.7	279.7	149.7	33.7	19.2	19.7	39.5	39.2	35.7	74.7
1315	124.7	299.7	154.7	34.6	19.7	20.7	41.2	41.7	37.9	79.7
1415	124.7	321.7	163.7	35.7	22.7	24.7	44.7	44.2	40.7	86.7
1525	131.7	340.7	184.7	41.2	23.7	24.7	48.0	47.5	43.8	92.5
1615	139.7	359.7	192.2	43.2	24.7	24.7	50.4	50.2	46.7	96.2
1715	153.0	380.7	204.7	44.7	26.7	28.2	54.6	54.2	50.2	102.7
1825	170.2	400.2	225.2	50.2	29.7	29.7	57.2	57.0	53.0	109.0

TABLE IV.- RAKE PRESSURES - Continued

(e) Test VI

p'_t, lb/sq in., abs	Rake pressures, lb/sq in., abs, at radius (in.) of -									
	0	0.5	1.0	1.5	2.0	2.5	0	0.5	1.0	1.5
	p'_p						p_A			p'_A
525	20.7	31.7	50.7	62.7	6.7	7.7	12.7	13.7	12.7	29.7
635	24.7	24.7	24.5	64.7	34.6	8.7	9.7	14.7	14.7	34.2
735	30.7	29.7	25.7	54.7	53.7	5.0	16.7	16.7	16.7	27.0
835	34.7	34.7	33.7	59.7	51.7	6.7	19.7	29.6	29.6	38.7
935	36.7	36.7	32.7	64.7	63.7	9.7	21.7	21.7	21.7	39.7
1015	40.7	40.7	40.7	74.7	74.7	9.7	23.7	23.7	23.6	48.2
1115	44.7	44.7	58.7	74.7	66.7	11.7	27.2	26.7	26.7	54.7
1235	49.7	48.7	51.7	92.7	79.7	12.7	29.2	28.7	28.7	57.7
1315	52.7	52.7	46.7	93.7	90.7	14.7	31.4	32.2	31.7	67.7
1415	56.7	56.7	59.2	102.2	103.7	14.7	32.4	35.2	35.2	73.2
1515	60.7	60.7	72.7	112.7	94.7	17.7	36.7	36.7	36.7	77.7
1615	64.7	64.7	59.7	113.7	115.2	13.7	38.3	37.7	38.2	75.7
1715	70.7	68.7	86.7	118.7	103.7	19.7	41.2	41.7	41.7	85.7
1815	74.7	74.7	71.7	132.2	26.7	18.7	43.2	43.2	43.5	89.2

(f) Test VII

p'_t, lb/sq in., abs	p'_p, lb/sq in., abs, at radius (in.) of -					
	0	0.5	1.0	1.5	2.0	2.5
535	20.7	20.7	20.7	34.7	40.7	7.7
645	25.7	25.7	46.7	34.7	10.7	14.7
735	29.7	29.7	50.7	39.7	23.7	17.7
795	32.7	32.7	54.7	43.7	22.7	18.7
915	36.7	36.7	58.7	47.7	24.7	20.7
1015	40.7	40.7	65.7	53.7	28.7	23.7
1115	44.7	44.7	74.7	58.7	33.7	25.7

(g) Test VIII

p'_t, lb/sq in., abs	Rake pressures, lb/sq in., abs, at radius (in.) of -									
	0	0.5	1.0	1.5	2.0	2.5	0	0.5	1.0	1.5
	p'_p						p_A			p'_A
535	21.7	21.7	34.7	74.7	6.7	7.7	11.7	11.7	9.7	29.9
640	25.7	25.7	35.7	20.3	14.7	6.7	16.7	15.7	14.7	40.2

TABLE IV.- RAKE PRESSURES - Concluded

(h) Test IX
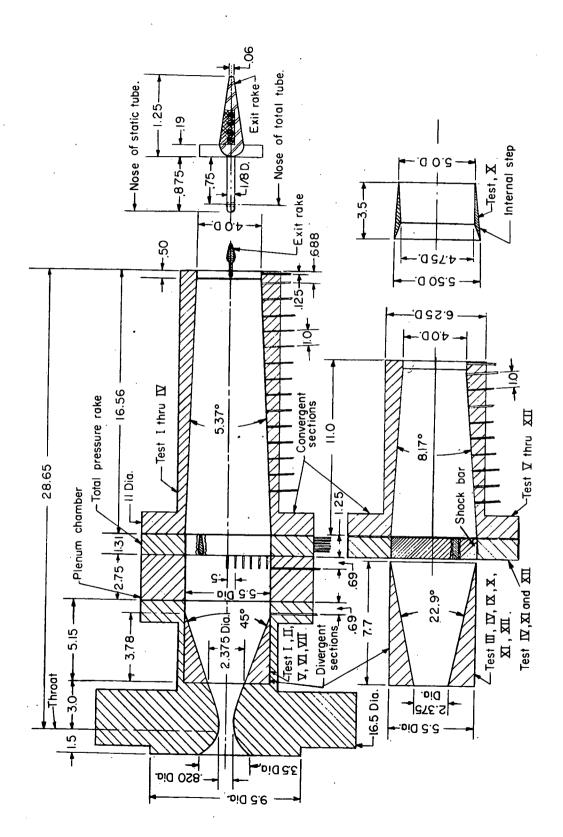
p'_t, lb/sq in., abs	p'_A, lb/sq in., abs, at radius (in.) of -			
	0	0.5	1.0	1.5
535	49.9	67.7	25.7	16.2
635	36.2	50.7	50.7	38.7
735	27.4	38.9	74.7	50.7
815	21.2	32.7	99.7	47.7
935	20.7	49.2	21.9	46.7
1015	20.7	57.7	112.7	70.2
1225	19.6	22.7	1.7	80.7
1335	20.2	21.2	2.7	40.7

(i) Test X

p'_t, lb/sq in., abs	p'_A, lb/sq in., abs, at radius (in.) of -			
	0	0.5	1.0	1.5
535	21.0	27.6	45.6	26.2
635	21.9	32.2	72.7	33.0
725	33.2	36.6	84.0	36.7

(j) Test XI

p'_t, lb/sq in., abs	p'_A, lb/sq in., abs, at radius (in.) of -			
	0	0.5	1.0	1.5
545	21.7	21.7	23.7	24.7
645	24.6	24.7	27.2	28.7
725	26.7	27.7	30.4	31.7
835	30.5	31.6	34.2	36.2
935	33.7	34.7	38.1	40.0
1025	36.7	38.2	41.7	44.7
1135	40.7	42.2	46.6	49.6
1225	43.9	44.8	50.4	52.9
1335	49.9	49.7	59.6	58.5
1435	50.8	52.8	58.8	62.7
1535	54.5	57.0	62.7	66.6
1615	56.8	59.9	66.7	70.7
1735	51.0	63.9	70.9	75.3
1825	64.2	66.1	75.3	80.4

Figure 1.- General layout of turbojet simulator and component parts. All dimensions are in inches.

NACA RM L57E10a

L-90661
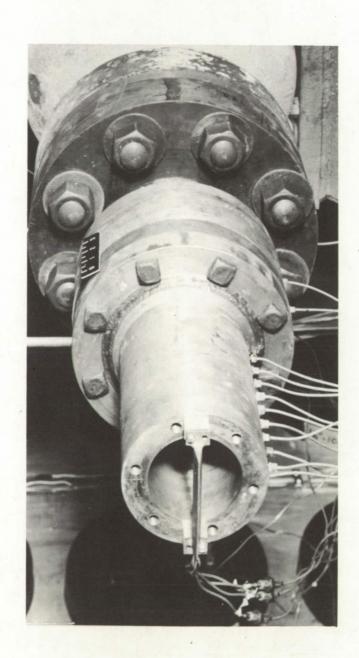
Figure 2.- Photograph of model of turbojet simulator in test position.

L-90659
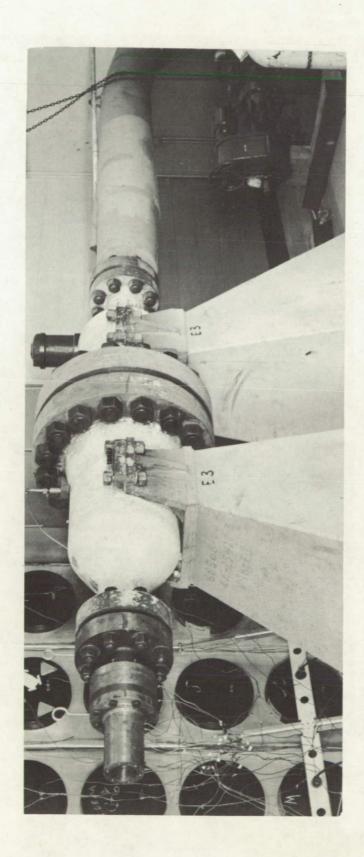
Figure 3.- Photograph of high-pressure tunnel used to test the model of the turbojet simulator.
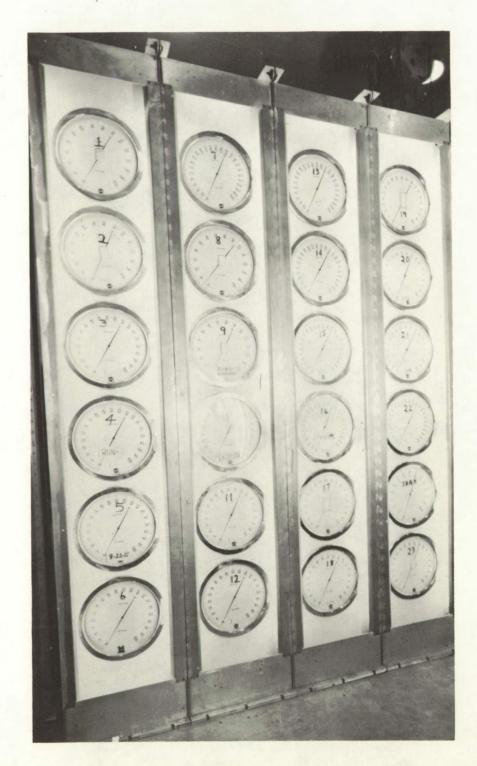
Figure 4.- Photograph of pressure-gage panel.   L-90665

Test I

Sonic

Q P

O N M L K J I H G F E D C B A

Test II

Sonic

Q P

O N M L K J I H G F E D C B A

Test III

Supersonic

O N M L K J I H G F E D C B A

Test IV

Sonic

O N M L K J I H G F E D C B A

(a) Test I to IV.
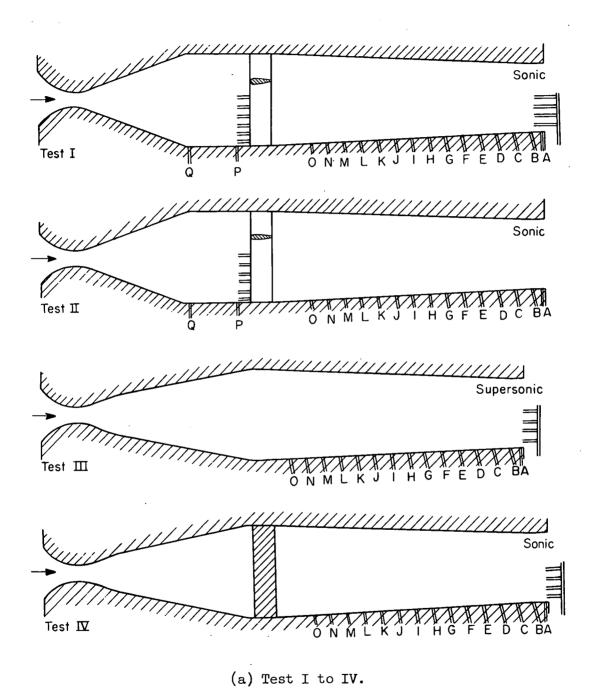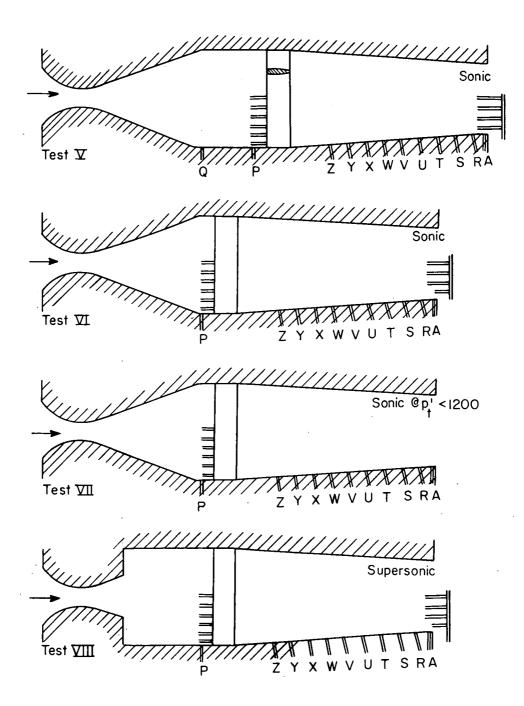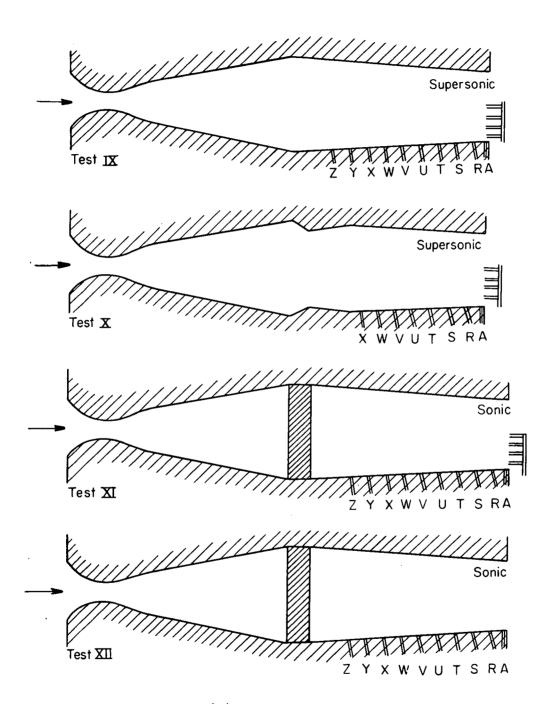
Figure 5.- Cross-sectional views of simulator configurations for tunnel
tests.

(b) Text V to VIII.

Figure 5.- Continued.

(c) Test IX to XII.

Figure 5.- Concluded.

L-90663
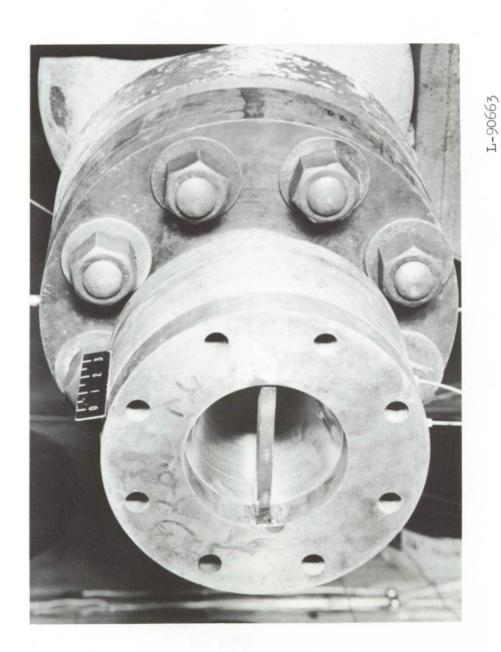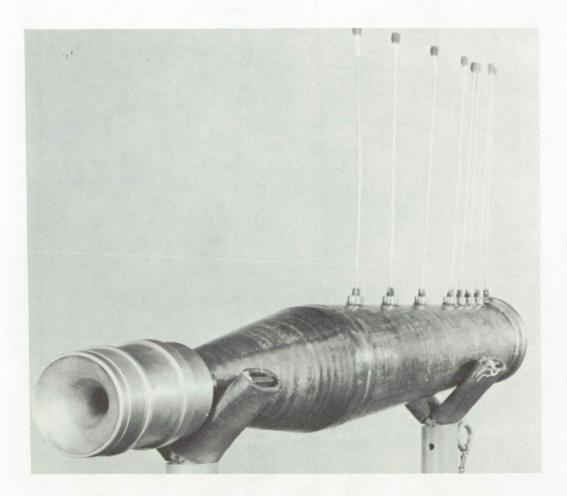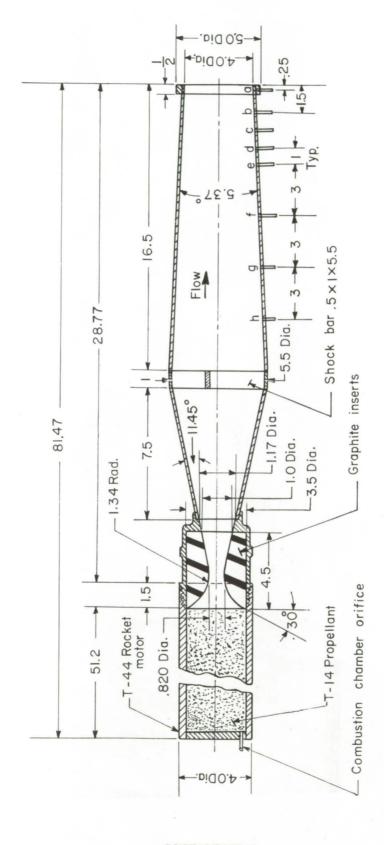
Figure 6.- Photograph showing internal bar in test position.

L-93202

Figure 7.- Photograph of turbojet simulator.

Figure 8.— Sketch of rocket motor with turbojet-exhaust simulator. (All dimensions are in inches.)
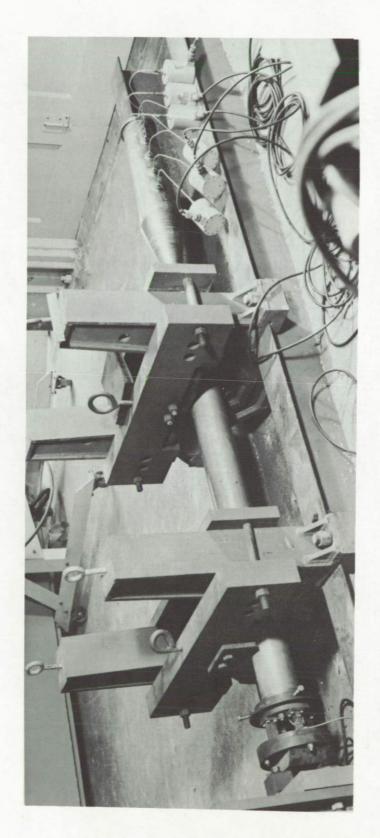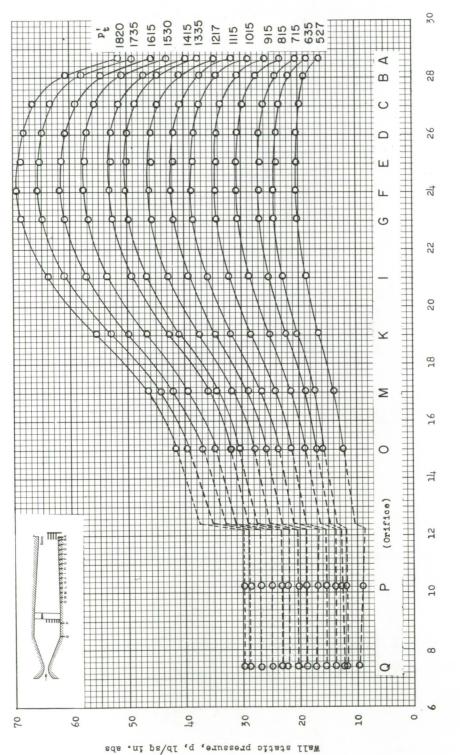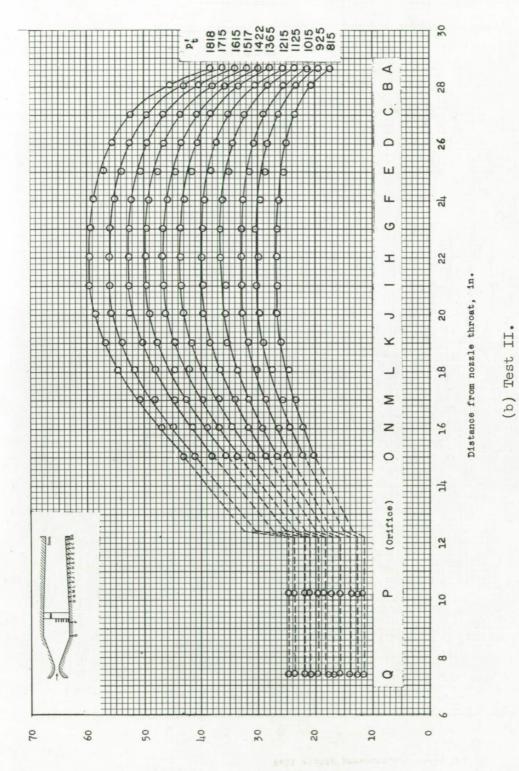
Figure 9.- Test setup of rocket motor and simulator. L-93354

Distance from nozzle throat, in.

(a) Test I.
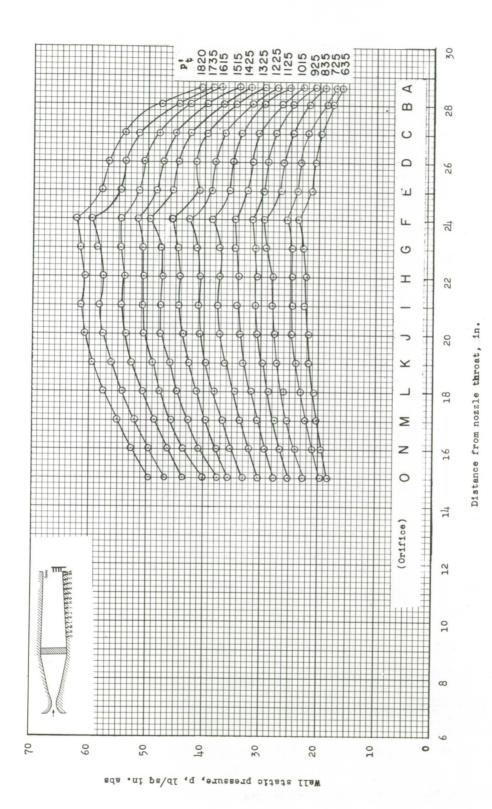
Figure 10.- Variation of static pressure along the turbojet simulator wall with tunnel total pressure for all sonic-exit tests.

(b) Test II.

Figure 10.- Continued.

p'$_t$
1820
1735
1615
1515
1425
1325
1225
1125
1015
925
835
725
635

Distance from nozzle throat, in.

Wall static pressure, p, lb/sq in. abs

(c) Test IV.

Figure 10.- Continued.

(d) Test V.

Figure 10.- Continued.

Distance from nozzle throat, in.

(e) Test VI.
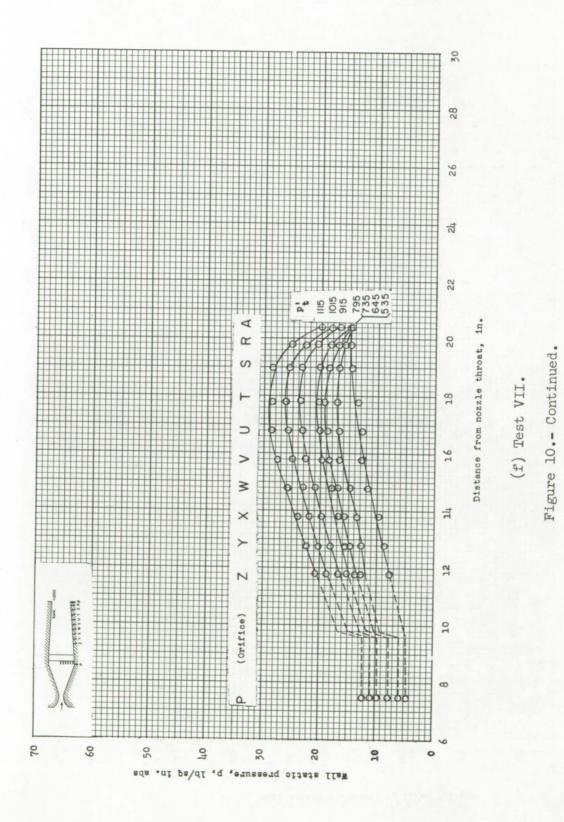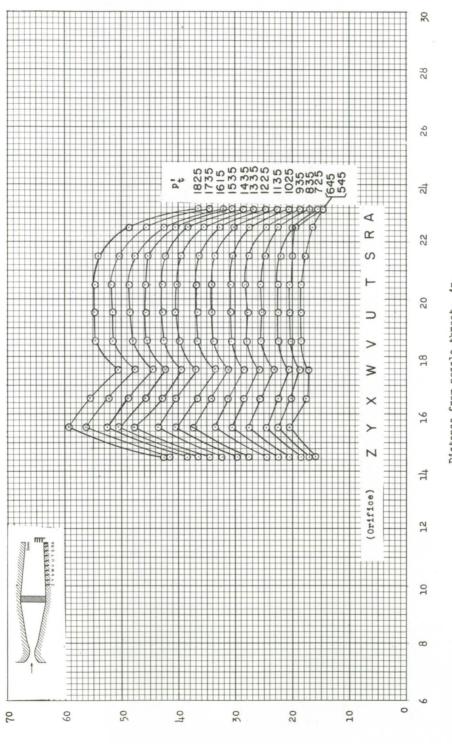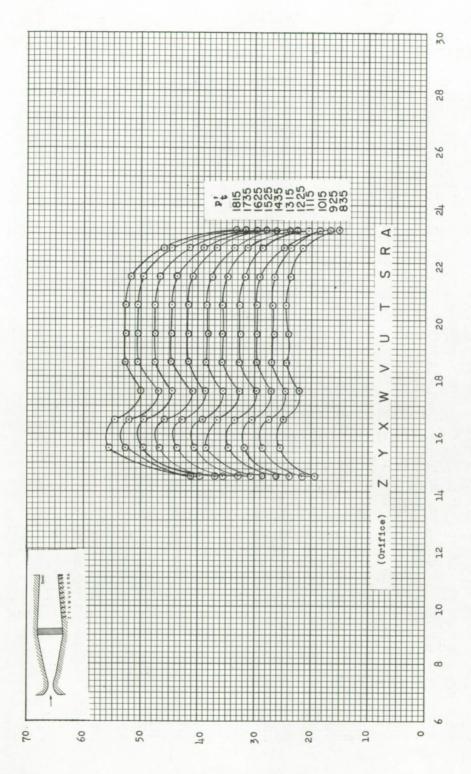
Figure 10.- Continued.

Wall static pressure, p, lb/sq in. abs

Distance from nozzle throat, in.

Wall static pressure, p, lb/sq in. abs

(f) Test VII.

Figure 10.- Continued.

(g) Test XI.

Figure 10.— Continued.

Distance from nozzle throat, in.

(h) Test XII.

Figure 10.- Concluded.
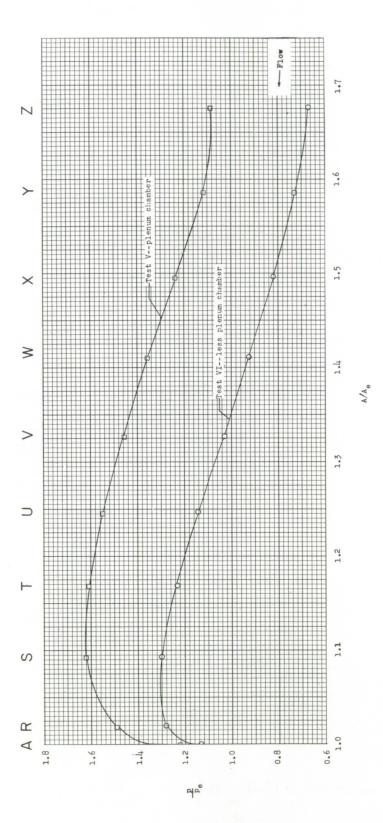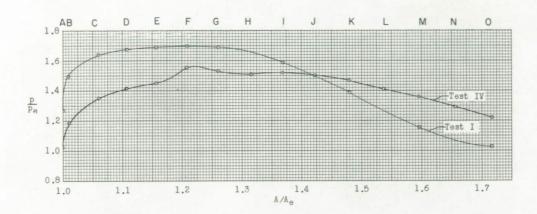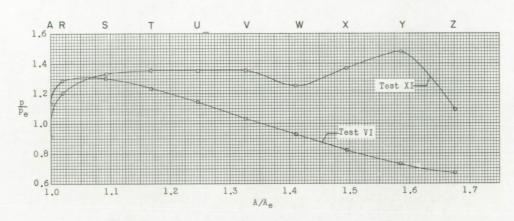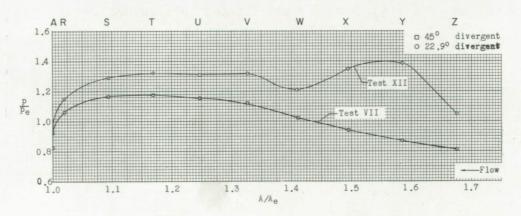
Figure 11.- Variation of wall-to-exit static pressure ratio with exit area ratio, showing effect of removing the plenum chamber. Both tests used 45° divergent and 8.17° convergent angles.

(a) Tests I and IV (5.37° convergence).
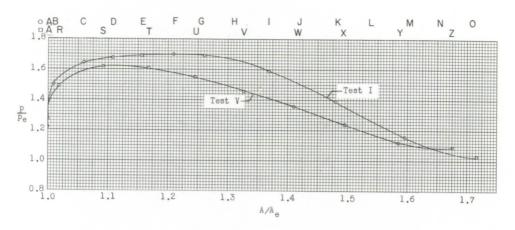
(b) Tests VI and XI (8.17° convergence).
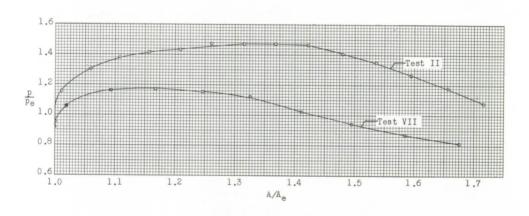
(c) Tests VII and XII (8.17° convergence).
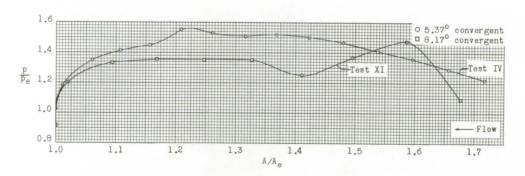
Figure 12.- Variation of wall-to-exit static pressure ratio with exit
area ratio for different divergence angles.

(a) Tests I and V (45° divergence).
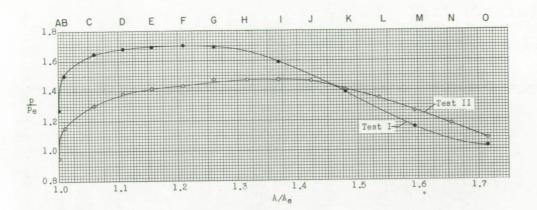
(b) Tests II and VII (45° divergence).
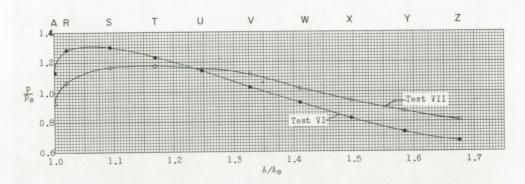
(c) Tests IV and XI (22.9° divergence).
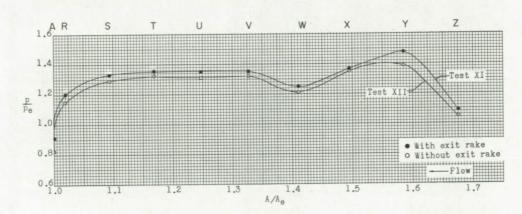
Figure 13.- Variation of wall-to-exit static pressure ratio with exit
area ratio for different convergence angles.

(a) Tests I and II (45° divergence) 5.37° convergence.
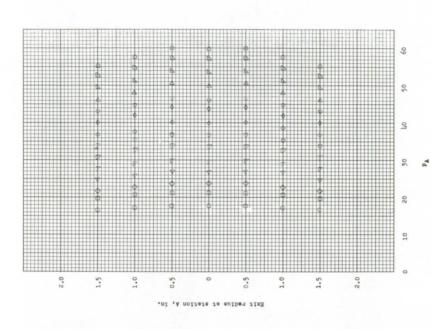
(b) Tests VI and VII (45° divergence) 8.17° convergence.

(c) Tests XI and XII (22.9° divergence) 8.17° convergence.

Figure 14.- Variation of wall-to-exit static pressure ratio with exit area ratio for tests with and without exit rake.

(a) Plenum chamber. (b) Exit.
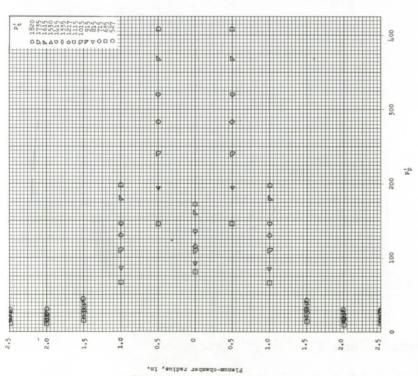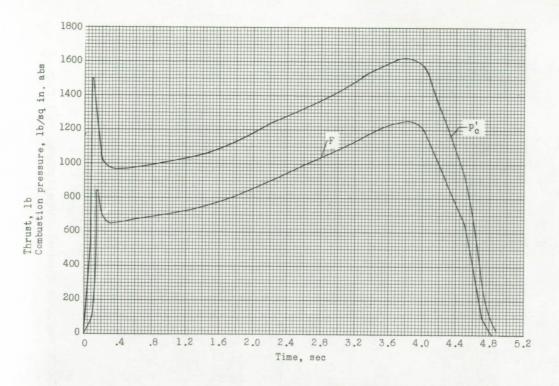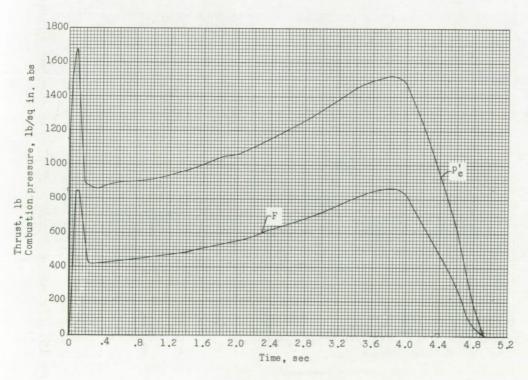
Figure 15.- Pressure survey of plenum chamber and exit for various tunnel total pressures for test I.

(a) Test 1 without shock bar.

(b) Test 2 with shock bar.

Figure 16.- Variation of combustion pressure and thrust with time from tests of the turbojet simulator with and without the shock bar.
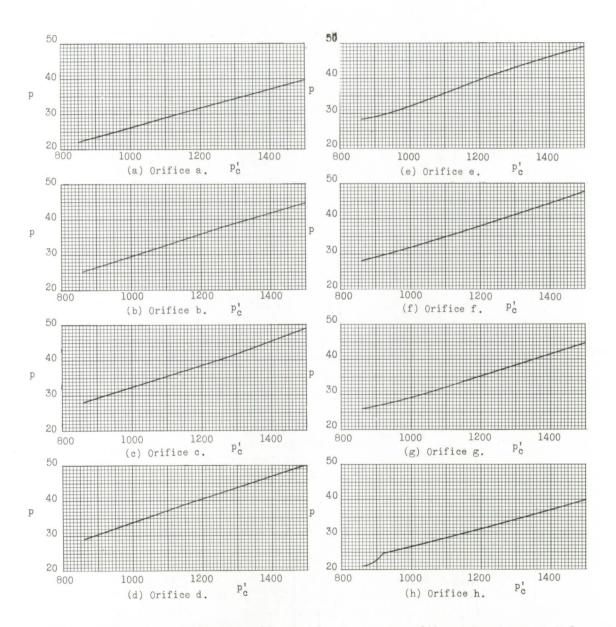
Figure 17.- Variation of wall static pressure with combustion total pressure for each orifice measurement on the turbojet simulator for the test with the shock bar.
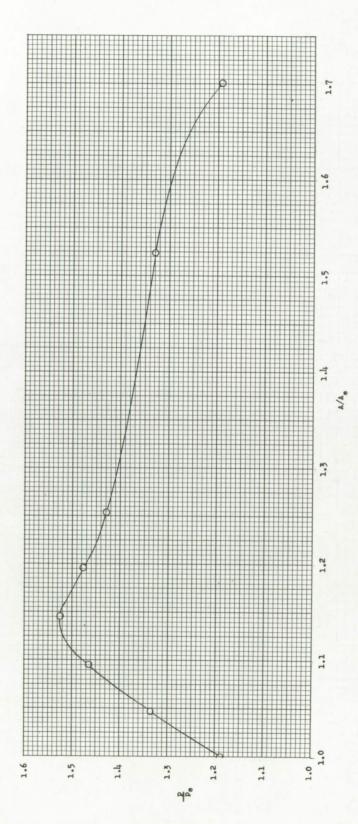
Figure 18.- Variation of wall-to-exit static pressure ratio distribution with exit area ratio for the turbojet simulator with shock bar.
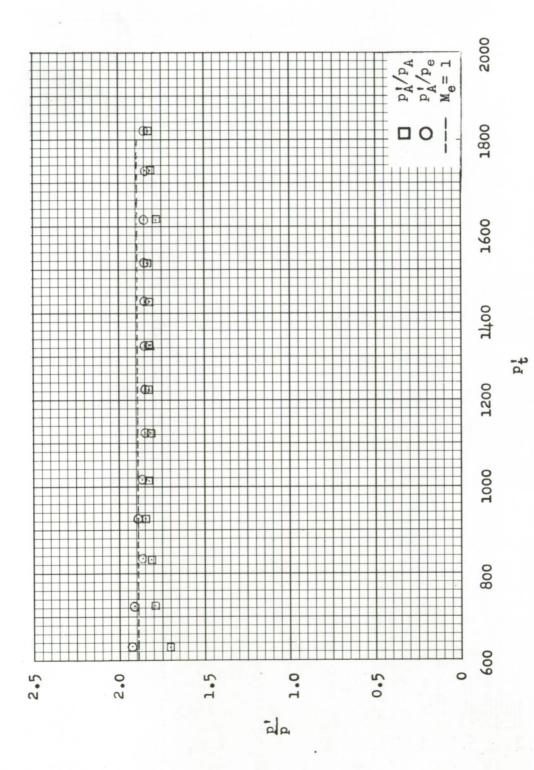
Figure 19.- Variation and comparison of total exit-pressure ratio with tunnel total pressure for both calculated p_e and measured p_A exit pressures.